ENGINEERING COMPUTATIONS, VOL. 11, 195–212 (1994)

A QUADRATIC ELEMENT FOR UPPER BOUND LIMIT ANALYSIS

H. S. YU, S. W. SLOAN AND P. W. KLEEMAN

Department of Civil Engineering and Surveying, The University of Newcastle, NSW 2308, Australia

ABSTRACT

This paper presents a new finite element formulation of the upper bound theorem. The formulation uses a six-noded linear strain triangular element. Each node has two unknown velocities and each corner of a triangle is associated with a specified number of unknown plastic multiplier rates. The major advantage of using a linear strain element, rather than a constant strain element, is that the velocity field can be modelled more accurately. In addition, the incompressibility condition can be easily satisfied without resorting to special arrangements of elements in the mesh. The formulation permits kinematically admissible velocity discontinuities at specified locations within the finite element mesh.

To ensure that finite element formulation of the upper bound theorem leads to a linear programming problem, the yield criterion is expressed as a linear function of the stresses. The linearized yield surface is defined to circumscribe the parent yield surface so that the solution obtained is a rigorous upper bound. During the solution phase, an active set algorithm is used to solve the resulting linear programming problem.

Several numerical examples are given to illustrate the capability of the new procedure for computing rigorous upper bounds. The efficiency and accuracy of the quadratic formulation is compared with that of the 3-noded constant strain formulation in detail.

KEY WORDS Finite element Limit analysis Plasticity Incompressibility Linear programming

INTRODUCTION

The upper bound theorem is often used to assess the stability of engineering problems by modelling the material with a perfectly plastic model obeying an associated flow rule. According to the upper bound theorem, the loads determined by equating the external rate of work to the internal rate of dissipation in a kinematically admissible deformation mode are not less than the actual collapse load. A velocity field is said to be kinematically admissible if it satisfies compatibility, the flow rule and the velocity boundary conditions. To provide solutions that are useful in practice, the upper bound theorem is often used in conjunction with the lower bound theorem. The lower bound theorem states that the loads, determined from a stress field that satisfies equilibrium, the stress boundary conditions, and the yield criterion, are not greater than the actual collapse load. With a suitable choice of the stress and velocity fields, the above two theorems enable the collapse load to be bracketed as closely as seems necessary for the problem under consideration.

Rigid block mechanisms have been used widely in the past to obtain useful upper bounds. In this approach, power is assumed to be dissipated only at the interfaces between adjacent blocks, and the geometry is optimized to yield the minimum dissipated power. A comprehensive discussion of the application of this technique for upper bound limit analysis may be found in

0264-4401/94/030195-18$2.00 *Received September 1992*

Reference 1. A major disadvantage of the use of rigid block mechanisms, however, is that they lack the ability to deal with problems involving complex loading and boundary conditions. To overcome this difficulty, finite element formulations of the upper bound theorem have been developed in recent years. Using these formulations, rigorous upper bounds can be determined by solving a linear programming problem[2,3,4,5]. The formulations permit localized plastic deformation to occur along velocity discontinuities, but also allow plastic deformation to occur throughout the material. Previously, a three-noded constant strain triangular element was used to model the velocity field, so that each node has two velocities and each element is associated with a set of non-negative plastic multiplier rates. To ensure that finite element formulation of the upper bound theorem leads to a linear programming problem, it is necessary to express the yield criterion as a linear function of the stresses. The linearized yield surface is defined to circumscribe the parent yield surface so that the solution obtained is a rigorous upper bound.

For a three-noded triangular element, it is necessary to use a special grid arrangement, in which four triangles are coalesced to form a quadrilateral with the central node lying at the centroid, so that the incompressibility condition can be satisfied throughout each triangle[6,7]. To remove this restriction, a higher order finite element formulation of the upper bound theorem is developed in this paper. The new formulation uses a six-noded linear strain quadratic triangular element. Each node has two unknown velocities and each corner of a triangle is associated with a specified number of unknown non-negative plastic multiplier rates. A major advantage of using a linear strain element, rather than a constant strain element, is that the velocity field can be modelled more accurately. Moreover, the incompressibility condition can be satisfied easily without resorting to the special element arrangement mentioned above.

Several relevant numerical examples are given to illustrate the capability and effectiveness of the new procedure for computing rigorous upper bounds. Detailed comparisons of efficiency and accuracy are made for the 3-noded constant strain formulation and the 6-noded linear strain formulation.

THEORY

The assumed velocity fields

Figure 1 shows the six-noded triangular element used for the upper bound formulation described in this paper. Each element is associated with twelve nodal velocities and $3p$ plastic multiplier rates (p is the number of sides in the linearized yield surface). The velocities are assumed to vary throughout each triangle according to:

$$u = \sum_{i=1}^{6} N_i u_i$$

$$v = \sum_{i=1}^{6} N_i v_i$$

where u_i and v_i are the nodal velocities in the x and y directions respectively and N_i are quadratic shape functions. The latter are defined as:

$$N_1 = \alpha(2\alpha - 1)$$

$$N_2 = \beta(2\beta - 1)$$

$$N_3 = \gamma(2\gamma - 1)$$

$$N_4 = 4\alpha\beta$$
$$N_5 = 4\beta\gamma$$
$$N_6 = 4\alpha\gamma$$

with

$$\begin{Bmatrix}\alpha\\ \beta\\ \gamma\end{Bmatrix} = \frac{1}{2A}\begin{bmatrix}a_i & b_i & c_i\\ a_j & b_j & c_j\\ a_k & b_k & c_k\end{bmatrix}\begin{Bmatrix}1\\ x\\ y\end{Bmatrix}$$

$$a_i = x_2y_3 - x_3y_2; \quad b_i = y_2 - y_3; \quad c_i = x_3 - x_2$$
$$a_j = x_3y_1 - x_1y_3; \quad b_j = y_3 - y_1; \quad c_j = x_1 - x_3$$
$$a_k = x_1y_2 - x_2y_1; \quad b_k = y_1 - y_2; \quad c_k = x_2 - x_1$$
$$A = \tfrac{1}{2}|(x_1 - x_3)(y_2 - y_3) - (x_3 - x_2)(y_3 - y_1)|$$

where A is the element area and $\alpha + \beta + \gamma = 1$.

Flow rule constraints for triangles

To use the upper bound theorem, a rigid–perfectly plastic material model with an associated flow rule is assumed. The plastic strain rates vary linearly throughout each triangle. For the Tresca criterion, it can be shown that the plastic flow rule will be satisfied everywhere within an element if we impose the flow rule at each corner of the element. The plastic flow rule at

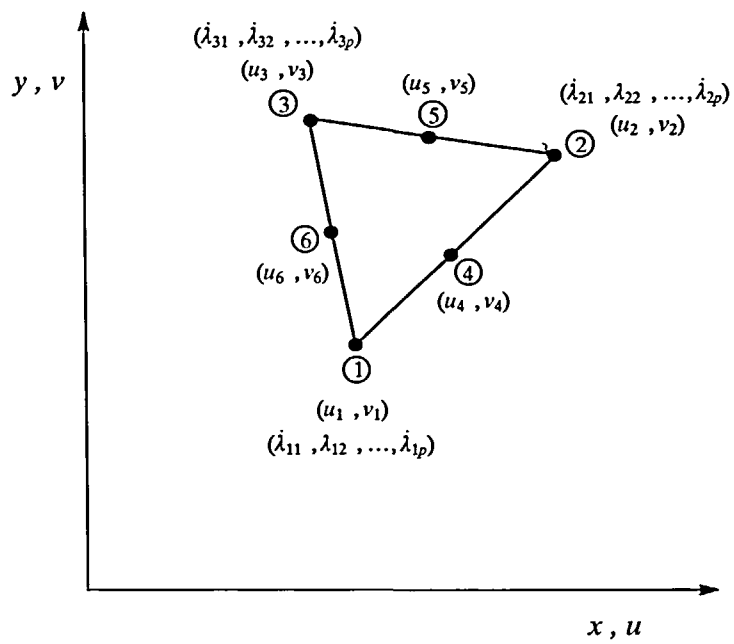

Figure 1 The six-noded linear strain triangular element for upper bound limit analysis

each corner node i can be expressed as:

$$\dot{\varepsilon}_{ix} = \left(\frac{\partial u}{\partial x}\right)_i = \dot{\lambda}_i \left(\frac{\partial F}{\partial \sigma_x}\right)_i \tag{1}$$

$$\dot{\varepsilon}_{iy} = \left(\frac{\partial v}{\partial y}\right)_i = \dot{\lambda}_i \left(\frac{\partial F}{\partial \sigma_y}\right)_i \tag{2}$$

$$\dot{\varepsilon}_{ixy} = \left(\frac{\partial u}{\partial y} + \frac{\partial v}{\partial x}\right)_i = \dot{\lambda}_i \left(\frac{\partial F}{\partial \tau_{xy}}\right)_i \tag{3}$$

and

$$\dot{\lambda}_i \geqslant 0 \tag{4}$$

where the superior dot denotes a derivative with respect to time, $\dot{\lambda}_i$ is a non-negative plastic multiplier rate associated with the corner node i, F is the yield function, and tensile strain is taken as positive.

When a linearization with p sides is used (see *Figure 2*), the Tresca yield criterion may be expressed as a linear function of the stresses according to:

$$F_k = A_k\sigma_x + B_k\sigma_y + C_k\tau_{xy} - 2c_u = 0$$

where plane strain loading is assumed and

$$A_k = \cos\alpha_k; \quad B_k = -\cos\alpha_k; \quad C_k = 2\sin\alpha_k$$

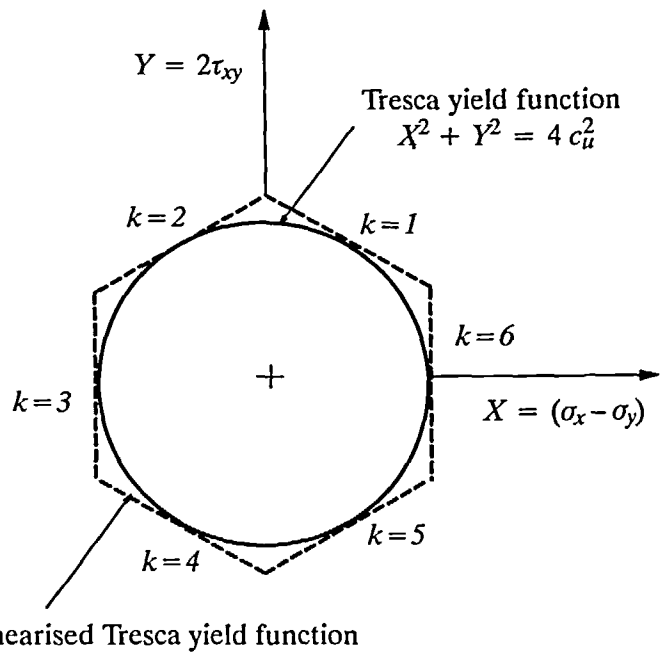

Figure 2 External linear approximation to Tresca yield surface ($p = 6$)

with

$$\alpha_k = \frac{2\pi k}{p}$$

Using the linearized yield function, the associated plastic flow rule (1)–(4) gives the plastic strain rates as:

$$\dot{\varepsilon}_{ix} = \sum_{k=1}^{p} \dot{\lambda}_{ik} \frac{\partial F_k}{\partial \sigma_x} = \sum_{k=1}^{p} \dot{\lambda}_{ik} A_k$$

$$\dot{\varepsilon}_{iy} = \sum_{k=1}^{p} \dot{\lambda}_{ik} \frac{\partial F_k}{\partial \sigma_y} = \sum_{k=1}^{p} \dot{\lambda}_{ik} B_k$$

$$\dot{\varepsilon}_{ixy} = \sum_{k=1}^{p} \dot{\lambda}_{ik} \frac{\partial F_k}{\partial \tau_{xy}} = \sum_{k=1}^{p} \dot{\lambda}_{ik} C_k$$

where $\dot{\lambda}_{ik}$ is the plastic multiplier rate associated with node i and the kth side of the yield surface. By using the displacement interpolation and differentiating the shape functions, the flow rule can be expressed as a set of equality constraints of the form:

$$\mathbf{a}_{11}\mathbf{u} + \mathbf{a}_{12}\dot{\boldsymbol{\lambda}} = \mathbf{b}_1 \tag{5}$$

where

$$\mathbf{a}_{11} = \begin{bmatrix} \left(\frac{\partial N_1}{\partial x}\right)_i & 0 & \cdots & \left(\frac{\partial N_6}{\partial x}\right)_i & 0 \\ 0 & \left(\frac{\partial N_1}{\partial y}\right)_i & \cdots & 0 & \left(\frac{\partial N_6}{\partial y}\right)_i \\ \left(\frac{\partial N_1}{\partial y}\right)_i & \left(\frac{\partial N_1}{\partial x}\right)_i & \cdots & \left(\frac{\partial N_6}{\partial y}\right)_i & \left(\frac{\partial N_6}{\partial x}\right)_i \end{bmatrix}$$

$$\frac{\partial N_j}{\partial x} = \frac{\partial N_j}{\partial \alpha}\frac{\partial \alpha}{\partial x} + \frac{\partial N_j}{\partial \beta}\frac{\partial \beta}{\partial x}$$

$$\frac{\partial N_j}{\partial y} = \frac{\partial N_j}{\partial \alpha}\frac{\partial \alpha}{\partial y} + \frac{\partial N_j}{\partial \beta}\frac{\partial \beta}{\partial y}$$

$$\mathbf{a}_{12} = -\begin{bmatrix} A_1 & A_2 & A_3 & \cdots & A_p \\ B_1 & B_2 & B_3 & \cdots & B_p \\ C_1 & C_2 & C_3 & \cdots & C_p \end{bmatrix}$$

$$\mathbf{u} = \{u_1, v_1, \ldots, u_6, v_6\}^T$$

$$\dot{\boldsymbol{\lambda}} = \{\dot{\lambda}_{i1}, \dot{\lambda}_{i2}, \ldots, \dot{\lambda}_{ip}\}^T$$

$$\mathbf{b}_1 = \{0, 0, 0\}^T$$

with $i = 1 \rightarrow 3, j = 1 \rightarrow 6$ and $k = 1 \rightarrow p$.

Thus the flow rule imposes nine equality constraints on the nodal velocities and plastic multiplier rates for each triangle. Each plastic multiplier rate is also subject to a non-negativity constraint.

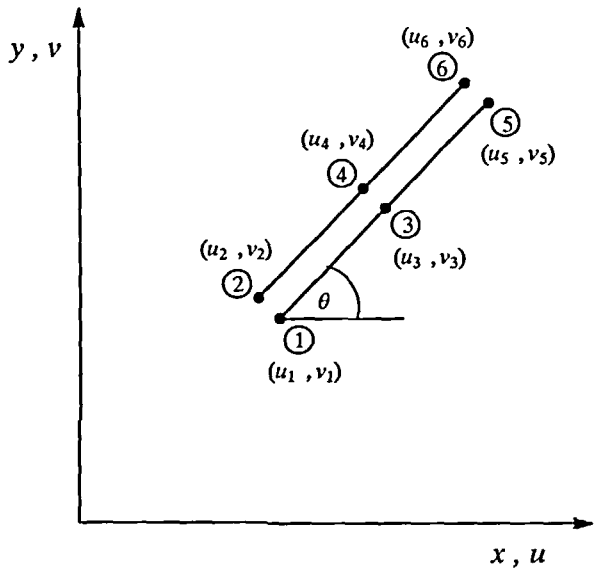

Figure 3 Velocity discontinuity

Flow rule constraints for discontinuities

In addition to allowing plastic deformation throughout each triangle, the upper bound finite element formulation also permits localised plastic deformation along velocity discontinuities. A typical segment of a velocity discontinuity, defined by the nodal pairs (1, 2), (3, 4) and (5, 6) is shown in *Figure 3*. For this arrangement, the jumps in tangential and normal velocities at the nodal pair (i, j) are given by

$$u_t^{ij} = \cos\theta(u_j - u_i) + \sin\theta(v_j - v_i)$$
$$u_n^{ij} = \sin\theta(u_i - u_j) + \cos\theta(v_j - v_i)$$

where ij denotes (1, 2), (3, 4) or (5, 6).

To preserve a linear constraint matrix in the formulation, it is necessary to specify the sign s of the tangential velocity jump such that $|u_t| = su_t$ and $s = \pm 1$. In order to ensure $su_t \geqslant 0$ along the discontinuity, we need to linearize the quadratic curve defined by su_t so that a linear programming problem can be obtained. If a 5-sided linearization is used (which is sufficiently accurate), it may be shown that the following six linear constraints are optimum in the sense that they constrain the velocity field by the least amount (see Appendix for the derivation):

$$su_t^{12} \geqslant 0$$
$$su_t^{34} \geqslant \tfrac{1}{4}(su_t^{56} - 5su_t^{12})$$
$$su_t^{34} \geqslant \tfrac{1}{8}(su_t^{56} - su_t^{12})$$
$$su_t^{34} \geqslant \tfrac{1}{8}(su_t^{12} - su_t^{56})$$
$$su_t^{34} \geqslant \tfrac{1}{4}(su_t^{12} - 5su_t^{56})$$
$$su_t^{56} \geqslant 0$$

These constraints can be written in the matrix form:

$$\mathbf{a}_2\mathbf{u} \leqslant \mathbf{b}_2 \tag{6}$$

where $\mathbf{a}_2$ is a simple function of θ and s, $\mathbf{b}_2 = \mathbf{0}$ and $\mathbf{u} = \{u_1, v_1, u_2, v_2, \ldots, u_6, v_6\}^T$. As well as satisfying a sign condition, the discontinuity velocities must also obey the flow rule. The assumption of a Tresca yield criterion implies that slip along a velocity discontinuity produces no dilation so that

$$u_n = 0$$

This flow rule constraint is satisfied everywhere along the discontinuity if we enforce it at each of the three nodal pairs, namely:

$$u_n^{ij} = 0$$

where ij denotes (1, 2), (3, 4) or (5, 6). The above linear constraint may be rewritten as:

$$\mathbf{a}_3\mathbf{u} = \mathbf{b}_3 \tag{7}$$

where $\mathbf{a}_3$ is a function of θ, $\mathbf{b}_3 = \mathbf{0}$ and $\mathbf{u} = \{u_i, v_i, u_j, v_j\}^T$.

Velocity boundary condition constraints

The last type of constraint to be imposed on the unknowns arises from the velocity boundary conditions. For a specified node i these conditions take the form $u_i = \delta_1$ and/or $v_i = \delta_2$, where δ_1, δ_2 are prescribed, and may be written in the following form:

$$\mathbf{a}_4\mathbf{u} = \mathbf{b}_4 \tag{8}$$

where $\mathbf{a}_4$ is the identity matrix, $\mathbf{u} = \{u_i, v_i\}^T$ and $\mathbf{b}_4 = \{\delta_1, \delta_2\}^T$.

Power dissipation in discontinuities

In the upper bound formulation, it is necessary to compute a kinematically admissible velocity field which minimises the internal power dissipation from both localised sliding along the velocity discontinuities and plastic deformation throughout the triangles.

The power dissipated along a velocity discontinuity of length L, per unit thickness in the out-of-plane direction, is given by:

$$P_d = \int_L c_u|u_t|\,\mathrm{d}L = sc_u \int_L u_t\,\mathrm{d}L$$

where $s = \pm 1$ is the specified sign of the discontinuity and c_u is the undrained shear strength. For the velocity discontinuity of *Figure 3*, the above integration may be performed analytically to give:

$$P_d = \frac{sc_uL}{6}(u_t^{12} + 4u_t^{34} + u_t^{56})$$

in which it is assumed that c_u is uniform throughout the mesh. This expression can also be written as:

$$\mathbf{P}_\mathrm{d} = \mathbf{c}_1^\mathrm{T}\mathbf{u} \tag{9}$$

where $\mathbf{c}_1$ is a function of s, c_u, L and θ, and $\mathbf{u} = \{u_1, v_1, \ldots, u_6, v_6\}^T$.

Power dissipation in triangles

The power dissipated by plastic deformation throughout each triangle may be written as:

$$P_t = \int_A (\sigma_x \dot{\varepsilon}_x + \sigma_y \dot{\varepsilon}_y + \tau_{xy} \dot{\varepsilon}_{xy})\, \mathrm{d}A$$

where a unit out-of-plane thickness is assumed and A is the triangle area. Substituting the expressions for the plastic strain rates and linearized yield function gives:

$$P_t = \frac{2c_u}{3} A \sum_{k=1}^{p} (\dot{\lambda}_{1k} + \dot{\lambda}_{2k} + \dot{\lambda}_{3k})$$

in which it is again assumed that the undrained shear strength c_u is uniform over a triangle. Alternatively, the above expression may be written in the matrix form:

$$\mathbf{P}_t = \mathbf{c}_2^{\mathrm{T}} \dot{\boldsymbol{\lambda}} \tag{10}$$

where $\mathbf{c}_2 = \dfrac{2Ac_u}{3}\{1, 1, \ldots, 1\}^T$ and $\dot{\boldsymbol{\lambda}} = \{\dot{\lambda}_{11}, \dot{\lambda}_{12}, \ldots, \dot{\lambda}_{1p}, \dot{\lambda}_{21}, \dot{\lambda}_{22}, \ldots, \dot{\lambda}_{2p}, \dot{\lambda}_{31}, \dot{\lambda}_{32}, \ldots, \dot{\lambda}_{3p}\}^T$.

THE UPPER BOUND LINEAR PROGRAMMING PROBLEM

All the equations that are necessary to formulate the upper bound theorem as a linear programming problem using finite elements have been developed in the preceding sections. For a given mesh, we now need only to assemble the various constraint matrices and objective function coefficients. The equations (5)–(10) developed above lead to the following linear programming problem:

$$\begin{aligned} \text{Minimize} \quad & \mathbf{C}_1^{\mathrm{T}}\mathbf{X}_1 + \mathbf{C}_2^{\mathrm{T}}\mathbf{X}_2 \\ \text{Subject to} \quad & \mathbf{A}_{11}\mathbf{X}_1 + \mathbf{A}_{12}\mathbf{X}_2 = \mathbf{B}_1 \\ & \mathbf{A}_2\mathbf{X}_1 \leqslant \mathbf{B}_2 \\ & \mathbf{A}_3\mathbf{X}_1 = \mathbf{B}_3 \\ & \mathbf{A}_4\mathbf{X}_1 = \mathbf{B}_4 \\ & \mathbf{X}_2 \geqslant \mathbf{0} \end{aligned}$$

where $\mathbf{X}_1$ is a global vector of unknown velocities and $\mathbf{X}_2$ is a global vector of unknown plastic multiplier rates.

In this paper, we employ duality theory in conjunction with the active set algorithm to solve the above linear programming problem. The active set method, which was recently developed[8], has been modified by Sloan[9] to improve its convergence and fully exploit sparsity. A detailed comparison of various strategies for solving the upper bound linear programming problem can be found in Reference 4.

NUMERICAL EXAMPLES

This section describes some applications of the new quadratic formulation of the upper bound theorem. A footing problem with a known closed form solution is analysed to investigate the accuracy of the numerical procedure. The effects of mesh refinement, approximation of the yield surface, and incompressibility constraints are studied in detail. The performance of the constant

strain 3-noded triangle is compared directly with the performance of the linear strain 6-noded triangle. To illustrate the application of the upper bound methods to a problem with no closed form solution, a trapdoor in a purely cohesive soil is also analysed.

Effects of incompressibility constraints

It is well known that conventional finite element computations using the displacement formulation with elastic–plastic models are often highly inaccurate in the fully plastic range[6,7,10]. These effects are caused by the excessive kinematic constraints that are imposed on the nodal velocities by a conflict between the plastic flow rule and the finite element discretization. This conflict arises when an incompressible plastic deformation mode, as defined by the plastic flow rule, cannot be modelled by the shape functions and the available degrees of freedom in the finite element mesh. In a collapse load calculation, too many incompressibility constraints may result in an over-stiff response. Several previous studies show that, for plane strain problems, only a few of the classical lower order elements are able to satisfy the incompressibility condition precisely. For axisymmetric problems, the situation seems to be much worse, as none of the common lower order elements are able to predict collapse loads accurately. Indeed it has been proved[7] that the linear strain triangle and the cubic strain triangle are the lowest order elements that are suitable for incompressible calculations under conditious of plane strain and axial symmetry respectively. As previously discussed[6], the incompressibility constraints may also be satisfied by using special arrangements of elements. In particular, the constant strain triangle can be used for plane strain incompressible calculations, provided the mesh is designed in such a way that four constant strain triangular elements are arranged to form a quadrilateral and its diagonals.

To investigate the performance of the 3-noded and 6-noded triangles, the meshes shown in *Figures 4* to *6* are used for the analysis of a smooth undrained footing problem. A vertical discontinuity at the edge of the footing is used in these meshes to allow localized plastic deformation to occur. In the first mesh, pictured in *Figure 4*, the 3-noded constant strain triangular

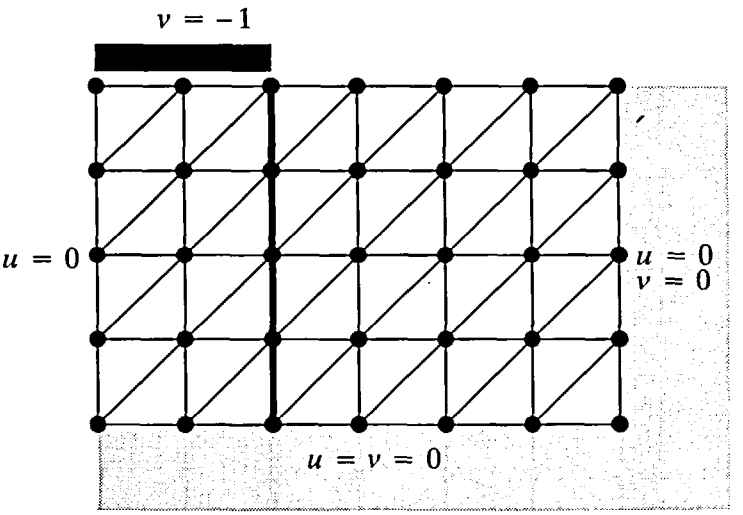

Figure 4 Mesh 1 – constant strain triangle without special arrangements of elements for modelling a rigid strip footing on a Tresca material

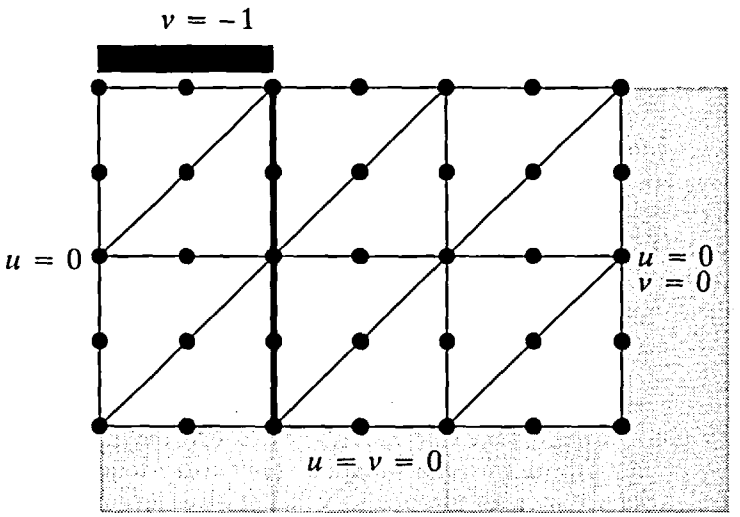

Figure 5 Mesh 2 – Linear strain triangle without special arrangements of elements for modelling a rigid strip footing on a Tresca material

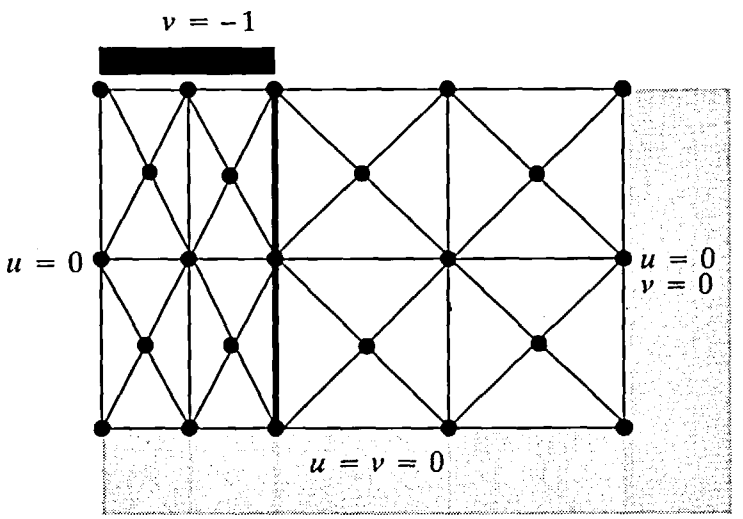

Figure 6 Mesh 3 – constant strain triangle with a special arrangement of elements for modelling a rigid strip footing on a Tresca material

element is used to model the displacement field. No special arrangement of the elements is used. The second arrangement is shown in *Figure 5*, and here the displacement field is modelled by the 6-noded linear strain triangular element. In the third arrangement, shown in *Figure 6*, the constant strain triangular element is again used but the grid is designed so that any quadrilateral is subdivided into four triangles with the central node located at the quadrilateral centroid.

In all calculations, the Tresca yield function is approximated using a 24-sided linearization. The degrees of freedom for Mesh 1, Mesh 2 and Mesh 3 are 80, 80 and 52, respectively. The

exact collapse load for a smooth rigid strip footing resting on a purely cohesive soil is given by the well-known Prandtl solution as $q_f = N_c c_u$, where c_u is the undrained shear strength and $N_c = 2 + \pi$. The errors in the collapse load for meshes 1, 2 and 3 are 37.5%, 8.3% and 12.5%, respectively. These results suggest that the 6-noded linear strain triangle can satisfy the incompressible condition without resorting to a special arrangement of the elements. The 3-noded constant strain triangle, on the other hand, is not generally suitable for incompressible calculations unless a special element arrangement, such as that used in Mesh 3, is employed. The theoretical prediction[6] is thus clearly applicable to the numerical upper bound procedures, even though it was developed for a traditional displacement type of finite element analysis.

Undrained loading of a smooth rigid strip footing

Figures 7–9 show three different meshes in which the 3-noded constant strain triangle is used to model the undrained collapse of a smooth rigid strip footing. In order to compare the performance of the 6-noded linear strain triangular element with the performance of the 3-noded constant strain triangle, meshes with the same number of degrees of freedom are used for both elements. The meshes for the 6-noded linear strain triangle are obtained from the meshes of *Figures 7–9* by using the simple transformation illustrated in *Figure 10*. This transformation ensures that the same number of degrees of freedom is obtained for the 3-noded constant strain element and the 6-noded linear strain element. The numerical results for the various analyses are presented in *Table 1*.

The numerical results for the 6-noded linear strain triangle and the 3-noded constant strain triangle suggest that the upper bound predictions are not particularly sensitive to the mesh refinement for this footing problem. The errors due to the approximation of the Tresca yield criterion are found to be negligible as long as at least 12 sides are used in the linearized yield surface. The results in *Table 1* also suggest that the 6-noded element gives very similar solutions to the 3-noded element, but typically requires less computer time. For meshes with the same

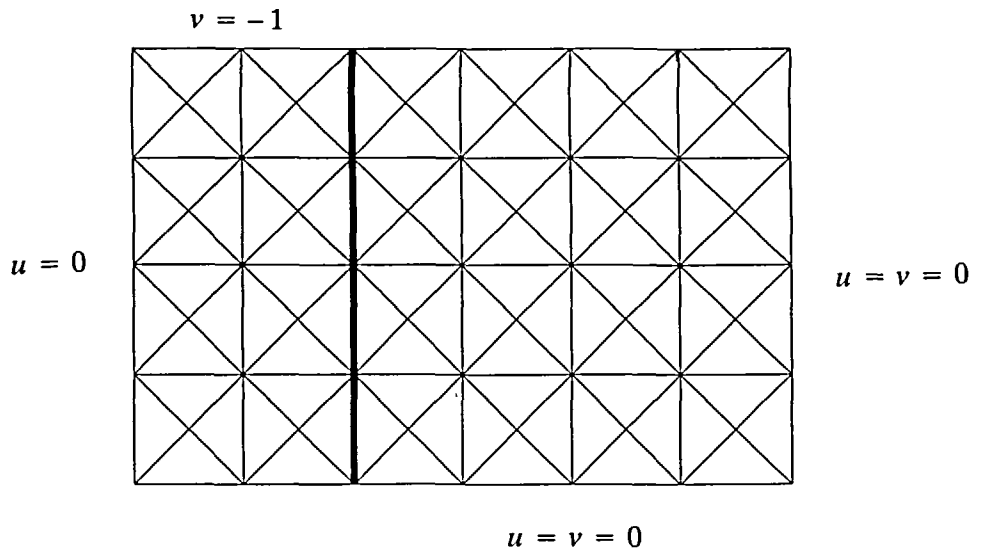

Figure 7 The coarse mesh used for modelling a rigid strip footing on a Tresca material

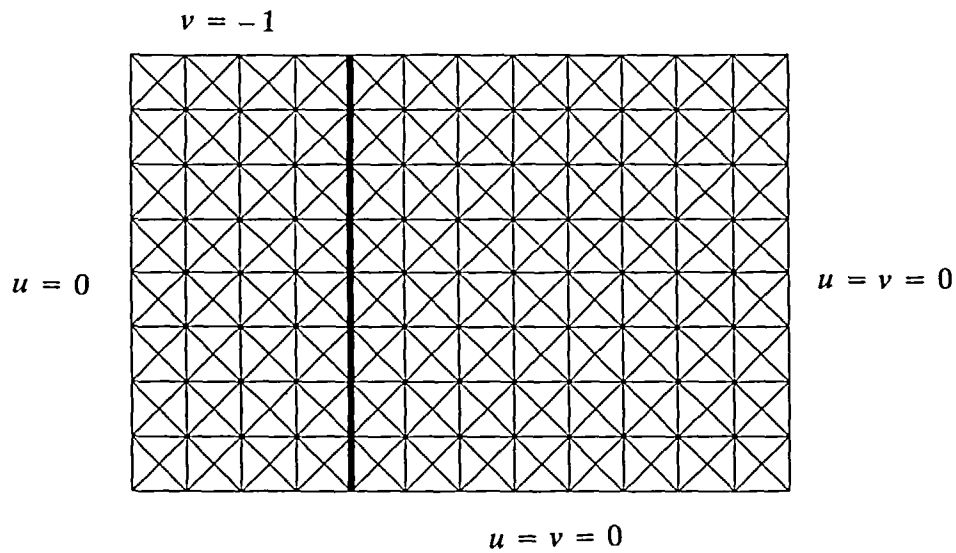

Figure 8 The medium mesh used for modelling a rigid strip footing on a Tresca material

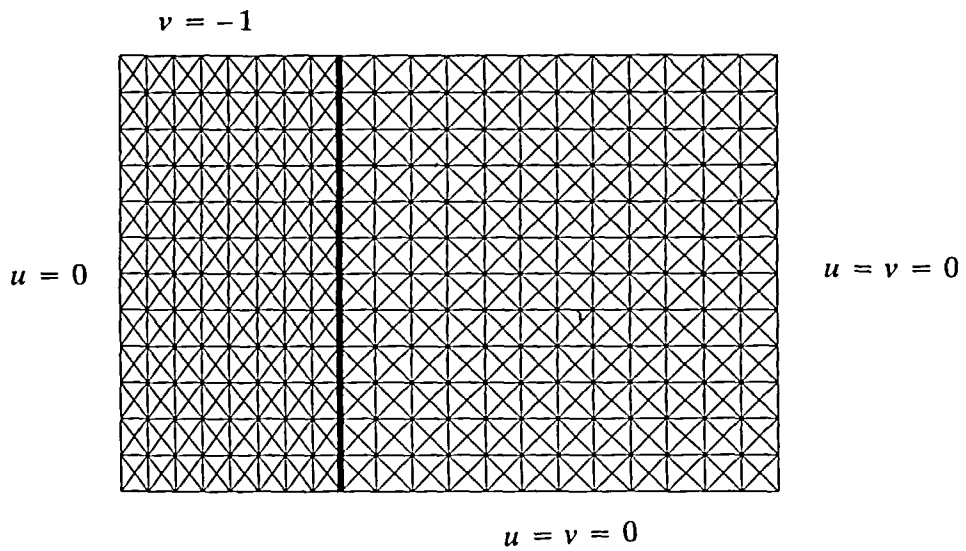

Figure 9 The fine mesh used for modelling a rigid strip footing on a Tresca material

number of nodes, the 6-noded formulation is generally more efficient than the 3-noded formulation because it leads to a smaller linear programming problem. This leads to a smaller number of iterations, and less CPU time, in the search for the optimum solution. For large problems with fine meshes, the 6-noded triangle is typically over 30 percent faster than the 3-noded triangle.

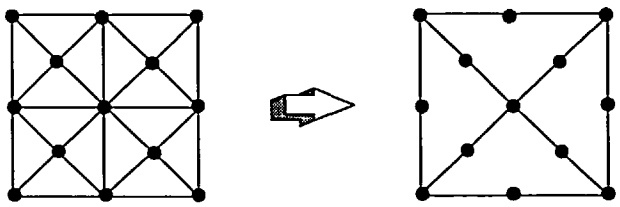

Figure 10 The scheme used for transforming a 3-noded triangle mesh into a 6-noded triangle mesh

Table 1 Results for smooth rigid strip footing on purely cohesive soil

		n		m		i		N_c		
p	Mesh	3-noded	6-noded	3-noded	6-noded	3-noded	6-noded	3-noded	6-noded	t_6^3
6	Coarse	329	263	709	571	192	144	5.63	5.64	1.09
	Medium	1227	951	2757	2193	969	770	5.50	5.49	1.11
	Fine	2995	2293	6825	5403	3528	2774	5.46	5.46	1.17
12	Coarse	329	263	1285	1003	254	234	5.44	5.53	0.95
	Medium	1227	951	5061	3921	1303	1000	5.31	5.34	1.19
	Fine	2995	2293	12585	9723	5307	3736	5.28	5.29	1.43
24	Coarse	329	263	2437	1867	370	320	5.39	5.47	1.05
	Medium	1227	951	9669	7377	1677	1650	5.27	5.29	0.97
	Fine	2995	2293	24105	18363	7270	5889	5.23	5.24	1.34

Notes:
p = number of sides in linearized yield surface
n = number of columns in overall constraint matrix
m = number of rows in overall constraint matrix
i = number of iterations for active set algorithm
t_6^3 = ratio of the CPU time for the 3-noded triangle and the 6-noded triangle

Undrained loading of a trapdoor

To illustrate the application of the proposed upper bound method to a problem with no closed form solution, the stability of a purely cohesive soil layer resting on a trapdoor is considered. The geometry of the problem, and the corresponding finite element mesh used in the analysis, are shown in *Figures 11* and *12* respectively. The grid has a vertical discontinuity at the edge of the trapdoor. The results for the upper bound analysis are given in *Table 2*, where the stability number is defined by $N = (\sigma_s + \gamma H - \sigma_t)/c_u$. Generally speaking, the results for the 6-noded linear strain formulation and the 3-noded constant strain formulation are very close, although the former tends to give slightly better solutions. As in the footing example, the 6-noded element is more efficient than the 3-noded element, and typically requires about 40 percent less CPU time.

CONCLUSION

A novel numerical method has been developed for computing rigorous upper bounds on limit loads. The procedure uses a 6-noded quadratic triangle and leads to a classical linear programming problem. The numerical results suggest that the proposed formulation is sufficiently accurate for practical calculations. When it is used in conjunction with a numerical formulation

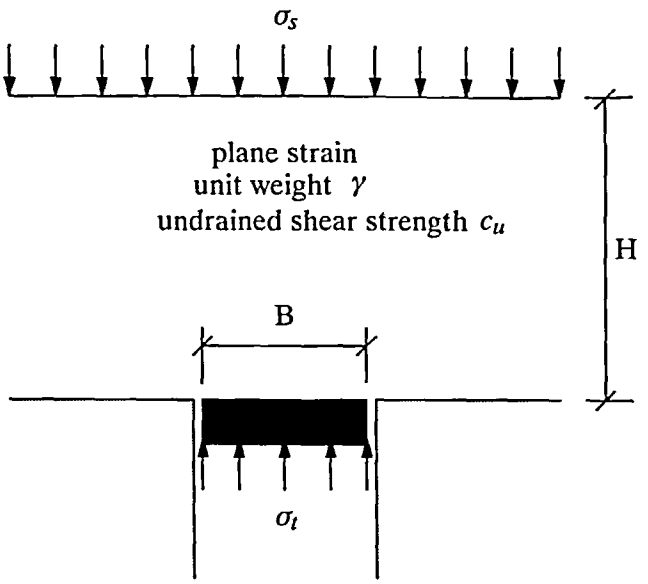

Figure 11 The trapdoor problem

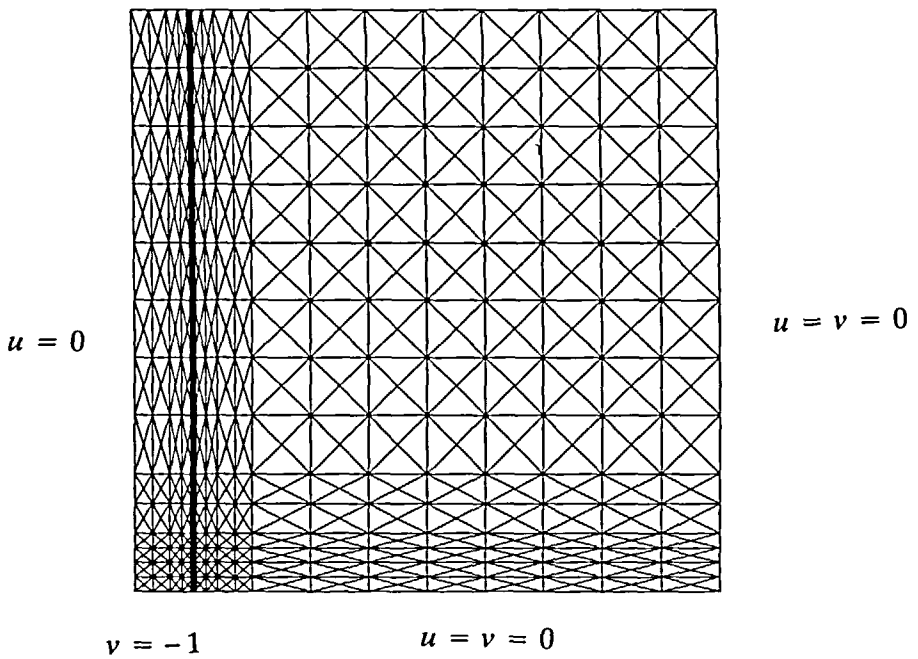

Figure 12 Mesh used for modelling a perfectly smooth trapdoor

Table 2 Results for trapdoor in a purely cohesive soil

	n		*m*		*i*		*N*		
p	3-noded	6-noded	3-noded	6-noded	3-noded	6-noded	3-noded	6-noded	t_6^3
6	2792	2141	6379	5056	2958	2136	6.79	6.70	1.23
12	2792	2141	11755	9088	4208	2852	5.42	6.41	1.42
24	2792	2141	22507	17152	6589	4750	6.33	6.33	1.40

Note: see *Table 1* for symbols

of the lower bound theorem[11], the method proposed in this paper can be used to provide accurate estimates of collapse. The numerical results suggest that the 6-noded linear strain triangle can, under conditions of plane strain, satisfy the incompressibility condition without resorting to a special element arrangement. The 3-noded constant strain triangle, on the other hand, tends to generate fewer degrees of freedom than incompressibility constraints and is therefore not suitable for incompressible calculations. All the results presented in this paper suggest that the performance of the 3-noded constant strain triangle can be significantly improved if a special arrangement of the elements is used. Generally speaking, the 6-noded linear strain formulation is more efficient than the 3-noded constant strain formulation.

ACKNOWLEDGEMENTS

The work reported in this paper forms part of a continuing research programme on stability analysis in the Department of Civil Engineering at the University of Newcastle. This research is supported by the Australian Research Council (ARC) and the authors are thankful for this support.

REFERENCES

1 Chen, W. F. *Limit Analysis and Soil Plasticity*, Elsevier, Amsterdam (1975)
2 Anderheggen, E. and Knopfel, H. Finite element limit analysis using linear programming, *Int. J. Solids Struct.*, **8**, 1413–1431 (1972)
3 Bottero, A., Negre, R., Pastor, J. and Turgeman, S. Finite element method and limit analysis theory for soil mechanics problems, *Comp. Meth. Appl. Mech. Eng.*, **22**, 131–149 (1980)
4 Sloan, S. W. Upper bound limit analysis using finite elements and linear programming, *Int. J. Num. Anal. Meth. Geomech.*, **13**, 263–282 (1989)
5 Yu, H. S. and Sloan, S. W. Upper bound limit analysis of a rigid plastic body with frictional interfaces, *Int. J. Mech. Sci.*, to appear
6 Nagtegaal, J. C., Parks, D. M. and Rice, J. R. On numerically accurate finite element solutions in the fully plastic range, *Comp. Meth. Appl. Mech. Eng.*, **4**, 153–177 (1974)
7 Sloan, S. W. and Randolph, M. F. Numerical prediction of collapse loads using finite element methods, *Int. J. Num. Anal. Meth. Geomech.*, **6**, 47–76 (1982)
8 Best, M. J. and Ritter, K. *Linear Programming: Active Set Analysis and Computer Programs*, Prentice-Hall, Englewood Cliffs (1985)
9 Sloan, S. W. A steepest edge active set algorithm for solving sparse linear programming problems, *Int. J. Num. Meth. Eng.*, **12**, 2671–2685 (1988)
10 Yu, H. S. A rational displacement interpolation function for axisymmetric finite element analysis of incompressible materials, *Finite Elements in Anal. and Design*, **10**, 205–219 (1991)
11 Sloan, S. W. Lower bound limit analysis using finite elements and linear programming, *Int. J. Num. Anal. Meth. Geomech.*, **12**, 61–77 (1988)

APPENDIX

Derivation of linear constraints for quadratic velocity discontinuity

With reference to *Figure A1*, the quadratic expression for the tangential velocity jump may be expressed by

$$u = ax^2 + bx + c$$

where a, b, c are constants.

The slope of the curve at any point may be evaluated using the following expression:

$$\frac{du}{dx} = 2ax + b$$

To linearise the quadratic curve, it is assumed that we start from the tangential lines which pass through the two end points C and E. It can be easily shown that the horizontal coordinate of the intersection point D is $\frac{x_1 + x_2}{2}$, where x_1 and x_2 are horizontal coordinates of the two end points C and E, respectively. The vertical coordinate of point D can also be shown to be:

$$u_D = ax_1x_2 + \frac{b}{2}(x_1 + x_2) + c$$

The area under the quadratic curve CFE is

$$Q_{ACFEB} = \frac{(x_2 - x_1)}{4}\left[\frac{4a}{3}(x_2^2 + x_1x_2 + x_1^2) + 2b(x_1 + x_2) + 4c\right]$$

and the area under the linearized curve CDE is

$$Q_{ACDEB} = \frac{(x_2 - x_1)}{4}(u_1 + 2u_D + u_2)$$

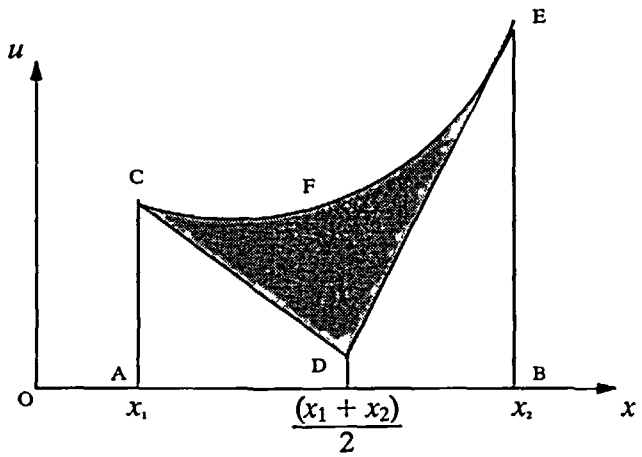

Figure A1 Three-sided linearization of a quadratic curve

where u_1, u_2 are the vertical coordinates of the two end points of the quadratic curve. The above equation can be further simplified to:

$$Q_{ACDEB} = \frac{(x_2 - x_1)}{4}[a(x_1 + x_2)^2 + 2b(x_1 + x_2) + 4c]$$

Hence the area for the area formed by CDEF should be

$$Q_{CDEF} = Q_{ACFEB} - Q_{ACDEB} = \frac{a}{12}(x_2 - x_1)^3$$

The above results can be used to find the optimum 5-sided linearization of the quadratic curve. As shown in *Figure A2*, a 5-sided linearization is obtained with five tangentials to points A, B, C, D and E whose horizontal coordinates are x_1, x_2, x_3, x_4 and x_5, respectively. The optimum linearization is defined here as the one that minimises the difference between the quadratic curve and the linearized approximation in terms of area.

Using the results obtained earlier, the area of this difference can be easily expressed in terms of x_1, x_2, x_3, x_4 and x_5 as follows:

$$Q = \frac{a}{12}[(x_2 - x_1)^3 + (x_3 - x_2)^3 + (x_4 - x_3)^3 + (x_5 - x_4)^3]$$

The conditions for the above area to be minimum are:

$$\frac{\partial Q}{\partial x_2} = 3(x_2 - x_1)^2 - 3(x_3 - x_2)^2 = 0$$

$$\frac{\partial Q}{\partial x_3} = 3(x_3 - x_2)^2 - 3(x_4 - x_3)^2 = 0$$

$$\frac{\partial Q}{\partial x_4} = 3(x_4 - x_3)^2 - 3(x_5 - x_4)^2 = 0$$

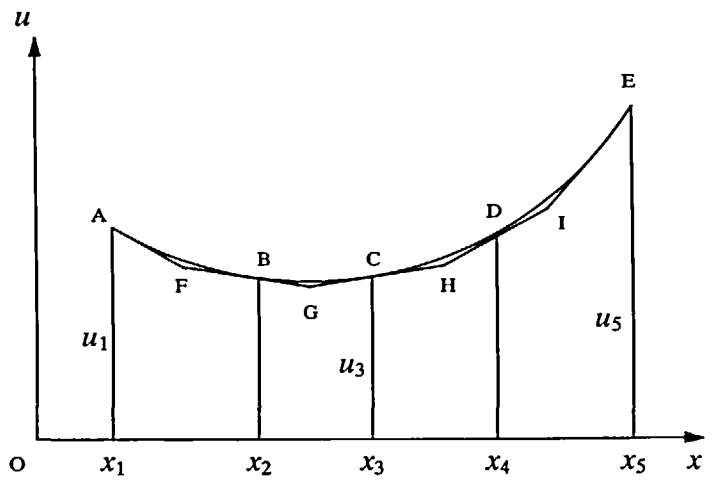

Figure A2 The least constrained five-sided linearization of a quadratic curve

which can be easily solved for x_2, x_3 and x_4. The solutions are:

$$x_3 = \frac{x_1 + x_5}{2}$$

$$x_2 = \frac{x_1 + x_3}{2}$$

$$x_4 = \frac{x_3 + x_5}{2}$$

To ensure that the vertical coordinates of all points of the quadratic curve are positive, we insist that the vertical coordinates of points A, F, G, H, I and E in *Figure A2* are positive. This gives six linear constraints on u_1, u_3 and u_5 which are vertical coordinates of points A, C and E respectively:

$$u_1 \geqslant 0$$
$$u_3 \geqslant \tfrac{1}{4}(u_5 - 5u_1)$$
$$u_3 \geqslant \tfrac{1}{8}(u_5 - u_1)$$
$$u_3 \geqslant \tfrac{1}{8}(u_1 - u_5)$$
$$u_3 \geqslant \tfrac{1}{4}(u_1 - 5u_5)$$
$$u_5 \geqslant 0$$

Replaciug u_1, u_3 and u_5 in the above inequalities with su_t^{12}, su_t^{23} and su_t^{56} gives the constraints on the tangential velocity jumps which ensure that su_t is positive everywhere on the discontinuity. Numerical experiments suggest that the five-sided linearization is sufficiently accurate for practical computations.